Optica Applicata, Vol. XIII, No. 1, 1983

Fiber-optic detectors

E. Beata Radojewska

Institute of Physics, Technical University of Wrocław, Wybrzeże Wyspiańskiego 27, 50-370 Wrocław, Poland.

Janusz M. Pawlikowski*

Institute of Energy Conversion, University of Delaware, Newark, DE 19711, USA.

A short review of the current state of the art of fiber-optic detectors is presented including design parameters for 1.3 μm-wavelength systems included. Experimental data of such detectors comprising technology data, operation modes and basic detector parameters are concisely discussed. Properties of the semiconductors used in optical-fiber transmission systems are also reviewed. Special attention is given to the properties and technology of ternary Ga(As, Sb) alloys. Finally, the proposal of high-efficiency fiber-optic detector made of graded-bandgap Ga(As, Sb) mixed crystal is discussed.

1. Introduction

The great explosion of fiber-optic technology and applications has been observed for several years. By substituting photons for electrons as the working particles and using glass fibers instead of metal wires as the transmitting medium we can easily get the highest speed (with lower costs) of data transferring ever obtained. Also, photonic devices are more efficient and more compact than the electronic ones. For instance, light-guiding-fiber-optical systems have functioned as normal telephone lines for several years [1].

This development has involved a progress in investigations of light sources (such as lasers, light emitting diodes, etc.) and of photodetectors. A special attention has been paid to 1.3 μm-wavelenght light emitting diodes [2–4] as well as to 1.3 μm-wavelength lasers, especially to heterojunctions ones [5]. Wavelength-range choice results from the properties of the light-guiding silica fibres. As shown in Fig. 1 the minimum attenuation exists at 1.2–1.3 μm-wavelength range for low-loss pure-silica fibres and their dispersion is also reduced to the minimum in this range [6]. An appropriate doping can shift the minimum attenuation to the longer-wavelength range, as in the case discussed in [7], where the lowest losses occurred in 1.6 μm-wavelength range. Great deal of effort has been also devoted to fabrication of 1.3 μm-wavelength photodetectors operating with optical fiber systems.

---

* On leave from the Institute of Physics, Technical University of Wrocław.

The first purpose of this report is to review briefly fiber-optic-detectors and to discuss the results published recently. Some advantages and disadvantages of a few types of photon detectors are pointed out and some properties of the used material are discussed. The next two chapters describe briefly the

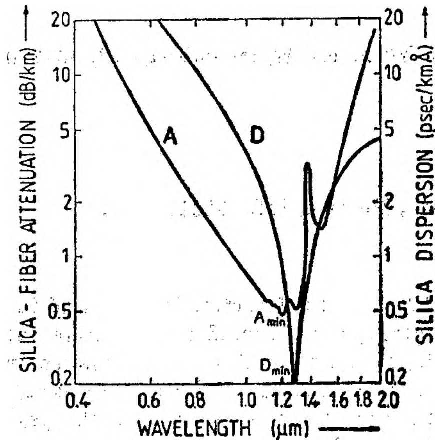

Fig. 1. Material dispersion and attenuation characteristics of a silica low-loss optical fibers, from [6]. A_{min} for $\lambda = 1.2$ μm, D_{min} for $\lambda = 1.27$ μm

basic types of photon detectors and their parameters. The other purpose of this report is to present the proposal of a high-efficiency 1.3 μm-wavelength graded bandgap photodetector, to discuss the material choice and to analyse its technological preparation possibilities.

2. Detector types

Visible and infrared radiation can interact with a solid state material in three ways: by thermal effects, photon effects and by wave interactions (see e.g. [8]) or in their combinations. The first group of the effects utilizes the cange of physical properties of solids caused by the temperature change due to absorption (so-called thermal detectors). In the second group of effects photons interact directly with electrons by transferring them the energy or the momentum (so-called photon detectors). The third group is based on the electromagnetic field interaction with a semiconductor causing a change in its field-dependent parameters. From that point of view an optical heterodyne detection may be classified among the third group of effects, despite the fact that it applies a photovoltaic or photoconductive detector [8].

Because of their common use only photon detectors exploiting internal photo-effects are described in this report. They can be divided into three classes, according to the origin of photoexcited carriers and their later behaviour. In the first class an incident photon having a sufficient energy interacts either with a valence-band electron or with a dopant, causing the respective generation of electron-hole or bound carrier-free opposite carrier pair. This class encloses the photocounductive, photovoltaic, photoelectromagnetic and Dember effects.

Interactions of incident photons with free carriers, e.g., photon drag and Putley effects belong to the second class, and in the third class incident photon excites a bound electron that is not able to leave the atom. This effect is utilized in infrared quantum counters and phosphors.

Some general conclusions can be inferred from the effect that is mainly employed in the detector operation principle. Photon detectors have, in general, shorter response times than the thermal ones, and moreover, they show a strong wavelength dependence of photoresponse per unit incident radiant power. Detectors with the long-wavelength cut-off, no longer than a few micrometers, can operate in room temperature, whereas the others should by cooled; the more extrinsic is the detector, the deeper cooling is needed [6, 9]. The fiber-optic detectors do not require a cooling operation, as a rule.

2.1. Photoconductive effect

Photoconductivity (PC) has been practically employed for many years, in the photonics as well. A typical photoconductive-detector operation circuit is shown in Fig. 2a. The conductivity change due to irradiation is a photoresponse source and can be expressed by the standard equation

$$\Delta\sigma = e(\mu_e \Delta n + \mu_h \Delta p) \qquad (1)$$

where μ_e and μ_h are mobilities of electrons and holes, respectively, and Δn and Δp are the respective concentrations of excess electrons and holes caused by the incident radiation. The photoresponse can be received either as changes in a potential difference on an extra resistor connected in series with the sample or as changes in the current flowing through the sample. In series added load resistance is often equal to the sample resistance, but that may involve non-optimal signal-to-noise ratio [8, 10].

2.2. Photovoltaic effect

Photovoltaic (PV) effect is the most often exploited in the area of question. It requires the existence of a potential barrier inside the semiconducting sample which can separate the generated electrons and holes. The barrier can be made by preparation of homojunctions, *p-i-n* junctions, heterojunctions, or Schottky-type junctions (Figs. 2b–e).

I–V characteristics of light-irradiated homojunctions are shifted with respect to those of non-irradiated ones and the shift is equal to the value of photocurrent I_{ph} when the junction is not biased (i.e. $U_B = 0$). These characteristics are described by the well-known equation

$$I = I_s\left[\exp\left(\frac{eU_B}{nkT}\right) - 1\right] - I_{ph} \qquad (2)$$

where I_s is the saturation current depending upon the material and junction parameters, and U_B is the applied bias voltage. In the simplest case the photo-

current is given by

$$I_{ph} = eA(L_e G_e + L_h G_h) \tag{3}$$

where L and G indicate diffusion length and generation rate, respectively (index e – for electrons, index h – for holes).

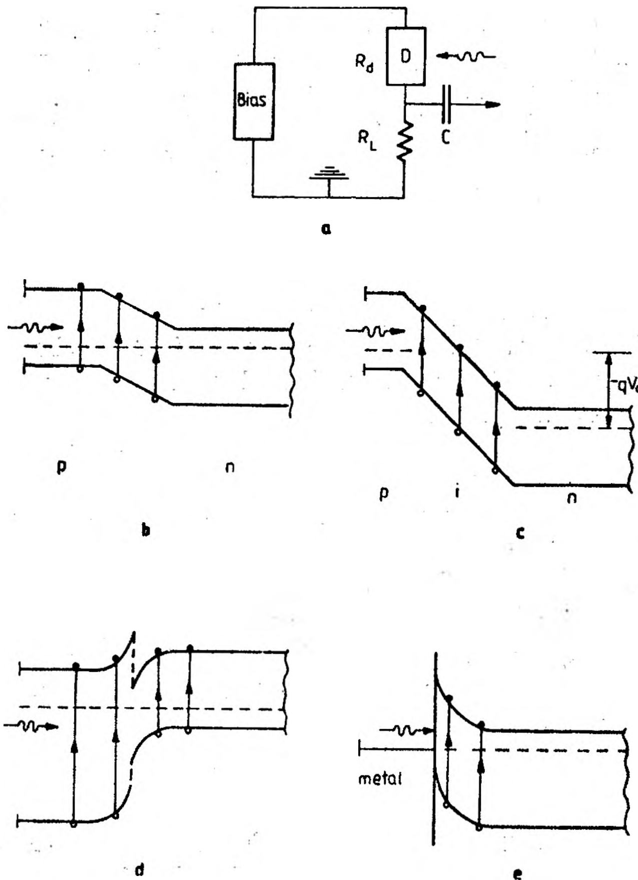

Fig. 2. Typical photo-conductive detector operation circuit (*a*), and photoexcitation processes in *p-n* homojunction (*b*), *p-i-n*-junction (*c*), hetero-junction (*d*), and metal-semiconductor (*e*)

The gradient of all band parameters (i.e., energy gap, carrier mobilities, their effective masses, etc.) in heterogeneous semiconducting materials (e.g., graded-bandgap mixed crystals) results in a bulk photovoltaic effect which may be also employed itself [11, 12] or used to amplify the other photoelectric effects [13].

An avalanche photodiode (APD) differs from the *p-n* photodiode mentioned above by an internal avalanche mechanism that occurs additionally. Therefore, signals coming from APD are higher than those from the described above junction diode made of the same material and operating under the same conditions. The avalanche effect does not improve the signal-to-noise ratio [8, 14], but is useful because of smaller requirements that must be fulfilled by an amplifier operat-

ing with the detector. Avalanche breakdowns occur in *p-n* junctions with lower dopant concentrations under reverse bias [8].

The *p-i-n* photodiode utilizes an extra intrinsic layer in between the two doped ones. If the irradiated layer is thin enough, radiation can reach this intrinsic area where electron-hole pairs may be generated. The intrinsic layer exhibits higher resistivity and breakdown voltage value than the neighbouring layers. Thus the reverse bias is present almost only in the intrinsic layer, producing high electric fields that involve the faster carrier drift.

An origin of photovoltaic effect in the Schottky junction is similar to that in the *p-n* junction and photoexcitation occurs in the depleted or neighbouring areas. In some semiconducting materials *p-n* homojunctions cannot be obtained at all, in the other cases only a few junctions exhibit a very good performance, so *p-n* junction can be easily substituted by a Schottky contact.

In the last decade heterojunction devices have been developed intensively. The improvement of various epitaxial techniques (e.g., MBE, VPE, OMVPE, LPE, LPEE) made it possible to obtain a number of semiconductor combinations. Semiconducting heterostructures show the composition-dependence of the energy gap in a large range. This enables the optimal choice of the absorbing-layer energy-gap in respect to the given wavelength. The devices described above seem to be the most promising ones in the future.

2.3. Photoelectromagnetic effect

The photoelectromagnetic (PEM) effect is rarely employed in a fiber-optic signal detection. It requires highly absorbing semiconducting materials in which the electron-hole pairs generated by the absorbed photons near the irradiated surface are separated due to the applied magnetic field during diffusion process. When the surface recombination may be neglected and the sample is relatively thick with respect to the carrier diffusion length, the electromative force obtained for weak radiant powers and weak magnetic fields can be expressed by standart equation

$$\mathrm{EMF}_{\mathrm{PEM}} = \frac{e\Gamma L(\mu_e + \mu_h)B}{\sigma}, \tag{4}$$

where Γ is the surface generation rate, L — the diffusion length, B — the applied magnetic field, and σ — the irradiated sample conductivity.

2.4. Dember effect

The effect has been found not to be useful enough in practical applications. It utilizes the presence of the internal electric field produced by the difference between mobilities of photoexcited electrons and holes. The photovoltage is low (of the order of kT/e) but can be increased by applying a heterogeneous semiconductor [13].

2.5. Putley effect

PUTLEY [15] has shown that photoexcitation of electrons from one Landau level to the next one may be caused by far-infrared photons due to the cyclotron resonance absorption in presence of the applied magnetic field. The effect has not yet been completely investigated and has not been applied in photonics.

2.6. Photon drag effect

The photon drag (PD) effect consists in a transferring photon momentum to a free electron. This effect has not found wide applications in fiber-optic technique because of its low spectral sensitivity. However, photon drag detectors function quite well in far-infrared [16], and since they can absorb high densities of radiant power, they are very useful, for instance, in laser-beam detection.

3. Basic detector parameters

The basic detector parameters were widely described previously (see e.g. [17]). They will be shortly presented below as an introduction to the next Section.

3.1. Spectral sensitivity

Spectral sensitivity describes the value of photovoltage ($U_{\rm ph}$) or photocurrent ($I_{\rm ph}$) per unit incident radiant power:

$$R_{\lambda,f} = \frac{U_{\rm ph} \text{ or } I_{\rm ph}}{P_{\lambda,f}}, \text{ (V/W or A/W)}, \tag{5}$$

where $P_{\lambda,f}$ is the incident radiant power. The sensitivity is usually not the basic parameter in photonic applications.

3.2. Noise equivalent power

Noises limit the detection of weak radiant signals and are generated inside the detector (Johnson-Nyguist noise, resistance noise, generation-recombination noise, etc.) as well as by an amplifier operating with the detector. Another source of noises is an ambient atmosphere. The noise equivalent power (NEP) is given by the following equation

$$\mathrm{NEP}_\lambda = P_\lambda \frac{U_N}{U_{\rm ph}}, \text{ (W)}, \tag{6}$$

where U_N is the total noise voltage.

3.3. Detectivity

Detectivity is a basic parameter in fiber-optic applications. As the detector operation is limited by noises, detectivity is a useful parameter which is independent of the detector area and the amplifier band (Δf), but depends upon the

detector and amplifier noises. For a given wavelength the detectivity is defined as

$$D_\lambda^* = \frac{(A\Delta f)^{1/2}}{\mathrm{NEP}_\lambda} = \frac{U_{\mathrm{ph}}}{U_N}\,\frac{(A\Delta f)^{1/2}}{P_\lambda},\ (\mathrm{cm\ Hz^{1/2}W^{-1}}) \tag{7}$$

3.4. Response time

Response time (τ_R) of a detector is mostly determined by the life-time of the minority carriers exploited in the detector. It involves also some requirements with respect to the parameters of the amplifier used in the detector circuit.

In some applications the response time is not of so big importance as in fiber-optic systems and integrated optics.

3.5. Signal-to-noise ratio

This very convenient parameter for an optical receiver is given typically (see e.g. [2]) by the formula

$$\mathrm{STN} = \frac{e(M_\eta P_S)^2}{2(\hbar\omega)^2\Delta f[(e\eta P_S/\hbar\omega)\,M^2F_S + I_{DM}M^2F_D + I_{DS} + I_E]}, \tag{8}$$

where e is the elementary charge, $\hbar\omega$ – the energy of photons, η – the quantum efficiency, I_{DM} – the multiplied dark current, I_{DS} – the non-multiplied dark current, I_E – the amplifier noise-equivalent current, P_S – the peak-signal power, Δf – the bandwidth. I_E is the noise contribution of the amplifier written usually as an equivalent current given by the double ratio of the effective-noise voltage of the amplifier and the resistivity of the load resistor. F_S and F_D are the excess noise factors pertinent to the avalanche multiplication of the signal and dark currents, respectively, and may be related to the multiplication factor (M), through the effective ratio of the hole-to-electron or electron-to-hole ionization coefficients (k_{eff})

$$F_{S,D} = Mk_{\mathrm{eff}} + (1-k_{\mathrm{eff}})\left(2-\frac{1}{M}\right). \tag{9}$$

It is easy to see that as a rule the low dark current and amplifier noise value are essential.

3.6. Amplifiers

Basic amplifier types currently being used in optoelectronic systems are shown in Fig. 3, after [2]. The simplest one (and commonly used) is the voltage amplifier with an input load resistor. Having a low-noise amplifier, the final noise will be the Johnson one of this resistor (typical value used is $R_L = 50$ ohm with total detector plus amplifier input and stray capacitance, C_t, of the order of some pF). In the second configuration a high-value R_L is used to reduce the noise and the resulting narrow bandwidth is compensated by an equalization

network $H(\omega)$. The third possesses the effective input resistance R_F/A, where A is an open-loop gain of the amplifier, where the noise contribution is reduced by factor of A and is the Johnson noise of R_F itself.

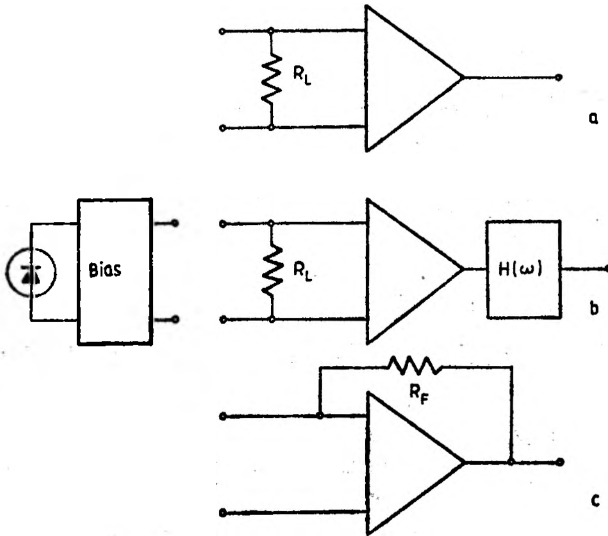

Fig. 3. The amplifier configuration frequently used in optoelectronic receivers: voltage-mode amplifier (a), equalized voltage-mode amplifier (b), current-mode amplifier (c)

The noise vs. bandwidth characteristics of the amplifiers discussed above are shown in Fig. 4, after [2]. The highest noise curve (a) is characteristic for voltage-mode amplifier having $R_L = 50$ ohm and $C_t \leqslant 3$ pF, as the typical values. The lower curve (a') represents the same mode with $C_t = 1.5$ pF and load resistor chosen to give a frequency response equal to the bandwidth. The lowest curve (b, c) represents the composition of measured and projected performances of

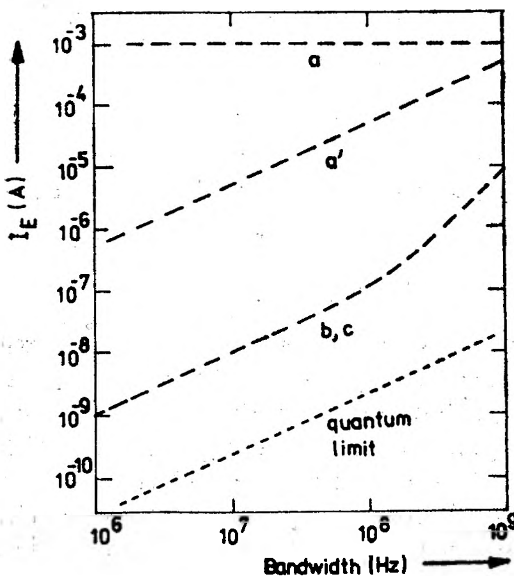

Fig. 4. I_E vs. bandwidth amplifier configurations from Fig. 5 (explanation – see the text)

equalized voltage-mode and current-mode amplifiers and shows the current state-of-the-art limit, assuming we are able to achieve very low total capacitance ($C_t < 1$ pF). For reference, there is also shown the quantum noise limit for a signal-to-noise ratio equal to 36, which corresponds to a bit error rate of 10^{-9} in a digital system.

3.7. "Ideal" detector

On the base of discussion in Sections 3.1–3.6 it is easy to formulate some requirements the "ideal" detector should fulfill. High sensitivity and low NEP (high signal-to-noise ratio) together with short response time (wide bandwidth) have set the design goal. There are, however, some limits connected mostly with material properties and technology of device. For instance, the high-speed and sensitive germanium detectors usually suffer from high dark current or multiplication noises.

From our viewpoint there is no substantial problem now to meet the goal of high-sensitivity and fast detector matched to the appropriate wavelength. The still existing problems are dark current and noises produced both by the detector and amplifier. The first problem has been solved when new materials and preparation methods have been applied (for a particular discussion – see next sections). The noises can also be reduced substantially when the hybrid integrated structure (the amplifier is packaged together with the detector) possessing very total capacitance ($C_t < 1$ pF) is used.

4. Materials and parameters

Recently, a great deal of attention in this matter has been devoted to ternary and quaternary semiconducting mixed crystals of $A_xB_{1-x}C$, $AB_{1-x}C_x$ and $A_xB_{1-x}C_{1-y}D_y$ types. They are discussed in Chapter 4.2. For comparative reasons, some "classical-semiconductor" detectors for this wave range are mentioned in Chapter 4.1.

4.1. Classical-semiconductor detectors

The term "classical-semiconductor" has been used here for both well-known semiconducting elements and binary semiconductors already widely utilized.

Some parameters of the binary-semiconductor detectors are shown in Table 1. Some other fragmentary details concerning GaAs and InSb detectors can be found in [18–21] and in [22], respectively. The fact that the radiation energy is not well fitted to the semiconductor energy gap involves a relatively low quantum efficiency of the detection, and the maximum photoresponse does not correspond to the range of the incident photon energy. Gallium arsenide exhibits too wide energy gap with respect to the optimal fiber-optic wavelength range, so to detect 1.2–1.3 μm-wavelength radiation the generation from

Table 1. Some parameters of binary-semiconductor detectors

Material	Operation mode	Operation range	Quantum efficiency	Others	Ref.
GaAs: : Cr	photoconductivity and PEM-effect	≃1.7 μm		$\tau_R = 1$ ms	[99]
GaAs- -Al	Schottky junction	0.8–1.2 μm	23%	$R_{\lambda,f} = 125$ A/W	[100]
InAs	*p-n* junction	0.5–3.5 μm	⩾ 25%	$\tau_R = 1$ μs	[101]
InSb	*p-n* junction	0.4–5.5 μm	⩾ 25%	$\tau_R = 5$ μs	[102]

impurity levels or photocarrier injection through Schottky barrier should be employed. Conversely, the energy gaps of InAs and InSb are being too narrow, the operation of the detectors made of these materials is based on the tail of the spectral characteristics. In this case the values of photoresponse depend strongly upon the state of the irradiated surface.

Data for Ge and Si photon detectors are shown in Table 2. The additional information is also given in [119–121]. It is worth noting that the results obtained for germanium are similar to those for ternary mixed alloys, which will be discussed in the next Chapter. The weak point of the multicomponent alloys is that the technology of their growth is more complex and not as well known as for germanium. However, Ge detectors have the high levels of dark current and high excess noise factor.

Table 2. Some parameters of Ge and Si detectors

Material	Operation mode	Operation range	Quantum efficiency	Others	Ref.
Ge	p-n^+ junction	0.4–1.55 μm	50%	$\tau_R = 120$ ps	[103]
Ge	*p-i-n* junction	1–1.65 μm	60%	$\tau_R = 25$ ns	[104]
Ge	p-n^+ junction	1–1.6 μm	50–100%	$\tau_R = 100$ ps	[105]
Si	*p-n* junction	1–1.3 μm			[106]

4.2. Ternary and quaternary mixed-crystal detectors

Detectors made of IV–VI mixed crystals (such as (Pb, Sn) Te and (Pb, Se) Se), though well known and operating quite well in far-infrared [23], cannot, however, be employed in near-infrared, since their energy gap is too small, and this implies that for the given wavelength the absorption coefficient is too high.

Among II–VI compounds, (Cd, Hg) Te is the only ternary mixed crystal that can be practically employed in near-infrared detection (see e.g. [24–27]), because its energy gap varies practically from zero (HeTe band structure is

inverted that gives the zero "thermal" energy gap) to 1.45 eV, at 300 K. This enables (Cd, Hg) Te detector to detect radiation within 0.85–30 μm-wavelength range. $Cd_{0.75}Hg_{0.25}Te$ and $Cd_{0.70}Hg_{0.30}Te$ have the maximal sensitivities for 1.27 μm at 300 K and 5–77 K, respectively.

III–V mixed crystals have found the most common application in 1.2–1.3 μm-wavelength photon detection. Since they exhibit composition-dependent energy gap, the latter can be chosen precisely in accordance with a given wavelength. Table 3 presents wavelength ranges that result from composition-

Table 3. Ternary-mixed crystals of III–V compounds

Material	Long-wavelength cut-off*, λ_0
co-cation	
In(P, Sb)	0.95–6.25 μm
In(P, As)	0.95–3.5 μm
Ga(P, Sb)	0.55–1.7 μm
Ga(As, Sb)	0.85–1.7 μm
co-anion	
(Al, In)Sb	0.75–6.25 μm
(Al, Ga)Sb	0.75–1.7 μm
(Al, In)As	0.55–3.5 μm
(Ga, In)As	0.85–3.5 μm

* λ_0(μm) ≃ 1.24/Eg (eV), approximately

dependent energy gaps for two extreme compositions, at 300 K. Figure 5 shows energy gaps versus composition to illustrate the data from Table 3. As it can be seen, some systems exhibit a specific bowing in the composition-dependent energy gaps.

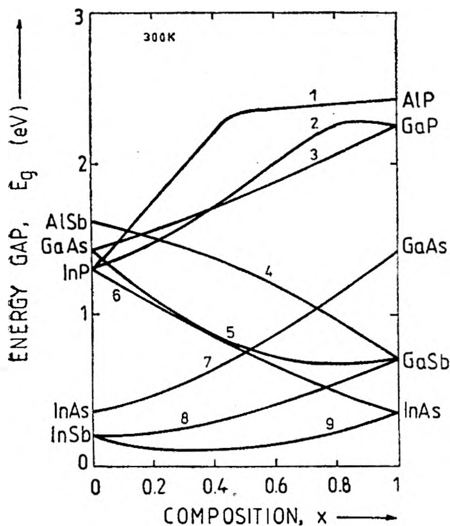

Fig. 5. Energy gaps of some III–V mixed crystals vs. molar composition, from [45, 61, 96–98]. 1 – $Al_xIn_{1-x}P$, 2 – $Ga_xIn_{1-x}P$, 3 – $GaAs_{1-x}P_x$, 4 – $Ga_xAl_{1-x}Sb$, 5 – $GaAs_{1-x}Sb_x$, 6 – $InP_{1-x}As_x$, 7 – $Ga_xIn_{1-x}As$, 8 – $Ga_xIn_{1-x}Sb$, 9 – $InSb_{1-x}As_x$

Recently, many papers have been devoted to (Ga, In) As and (Al, Ga) Sb mixed-crystal detectors for a 1.2–1.3 μm-wavelength range. Some parameters of these detectors are given in Tables 4 and 5. Other fragmentary details concerning (Ga, In) As and (Al, Ga) Sb can be found in [28-34] and in [35, 36], respectively. Both these materials were grown using mainly liquid-phase epi-

Table 4. Some parameters of (Ga, In)As detectors

Material	Operation mode	Operation range	Quantum efficiency	Others	Ref.
$Ga_{0.7}In_{0.3}As/GaAs$ (mesa)	*p-i-n* junction	≃ 1.15 μm	80%	τ_R = 10 ns	[107]
$Ga_{0.47}In_{0.53}As/InP$ (LPA)	*p-n* heterojunction	1–1.1 μm	65%		[108]
$Ga_{0.47}In_{0.53}As/Ga_{0.47}In_{0.53}As/InP$ (LPE, mesa)	p^+-*n*-n^+ junction	1–1.6 μm	60%	τ_R = 250 ps	[109]

taxial technique (LPE). Time response of these detectors is as short as a few hundreds of pikoseconds. It is worth mentioning that in these structures the avalanche mechanism is commonly employed. III–V compound devices which have the *p-n* junction located in the narrow-gap photo-sensitive layer are commonly characterized by high values of the dark currents at biases sufficient to achieve gain, which degrades the SNT parameter and limits the gain.

There are among the ternary III–V mixed crystals other three semiconducting alloys that for a certain composition exhibit near-1-eV-energy gaps. These are Ga(As, Sb), (Al, In)Sb and In(P, As). So far, however, no data on detector of these alloys have been published for the mentioned 1.2-1.3 μm-wavelength range.

The quaternary mixed-crystal detectors are dominated by III-V compounds. They exhibit the best attainable performance. The parameters of (In, Ga) (As, P) detectors are listed in Table 6. Some other fragmentary details can be found in [37-39]. Table 7 contains the parameters of (Ga, Al), (As, Sb) detectors, some information can be also found in [40].

In practice to prepare a detector the following two configurations: mesa and planar can be used. Figure 6 presents a quaternary detector [41] prepared by a mesa technique and its band diagram. The detector prepared by a planar technique [42] and its band diagram are shown in Fig. 7. The former detector has the active layer separated from the top surface by a window that exhibits a wider energy gap than the active layer, whereas in the planar-type detector the active layer is constituted by the top absorbing layer, where the photocurrent is affected by recombination due to surface states. The separation of generated photocarriers takes place there in homojunction. In the mesa-type detector this separation occurs in a heterojunction which possesses lattice defects, chemical disorder, recombination traps, etc.

Table 5. Some parameters of (Al, Ga)Sb detectors

Material	Operation mode	Operation range	Quantum efficiency	Others	Ref.
$Ga_xAl_{1-x}Sb/GaSb$, different values of x (LPE)	heterojunction	1–1.8 μm	≃60%	τ_R = 180 ps	[40]
$Ga_{0.52}Al_{0.48}Sb/Ga_{0.84}Al_{0.16}Sb/GaSb$, (mesa, LPE)	p^+-n-n^+ heterojunction	1–1.4 μm	60%	τ_R = 120 ps	[37]
$Ga_{0.3}Al_{0.7}Sb/GaSb$, (planar, LPE)	heterojunction	1–1.7 μm	54%		[110]

Table 6. Some parameters of (In, Ga), (As, P) detectors

Material	Operation range	Operation mode	Quantum efficiency	others	Ref.
InGaAsP/InP, (mesa, epitaxy)	p-n heterojunction	1–1.3 μm	54%	$R_{\lambda,f}$ = 0.46 A/W	[111]
$In_{0.84}Ga_{0.16}As_{0.34}P_{0.66}/InP$, (mesa, LPE)	p-n heterojunction	1–1.3 μm	54%	$R_{\lambda,f}$ = 0.46 A/W	[112]
$In_{0.84}Ga_{0.16}As_{0.34}P_{0.66}/In_{0.84}Ga_{0.16}As_{0.34}P_{0.66}/$ /InP, (mesa, planar, LPE)	p^+-n-n^+ homo- and heterojunctions	0.95–1.2μm	65%		[42]
$InP/InGaAsP/InGaAsP_3InP/InP$ (mesa, LPE)	p^+-p-n-n-n^+ homo- and heterojunctions	1–1.3 μm	70%	$R_{\lambda,f}$ = 0.5 A/W	[113]
InP/InGaAsP/InP (mesa, LPE)	p-n-n^+ heterojunction	0.9–1.7 μm 1.2–1.4 μm	50–70%		[41] [114]
InGaAsP/InP (mesa, planar) InGaAsP/InGaAsP/InP/InP (mesa, LPE)	p^+-n-i-n^+ homo- and heterojunction	0.9–1.3 μm	63%	τ_R = 100 ps	[115]
InGaAsP/InP		≃1.15	≃40%		[116]

Table 7. Some parameters of (Ga, Al), (As, Sb) detectors

Material	Operation range	Operation mode	Quantum efficiency	Others	Ref.
$Ga_{0.58}Al_{0.42}As_{0.02}Sb_{0.98}/Ga_{0.84}Al_{0.16}Sb/GaSb$ (mesa, LPE)	p^+-n-n^+ heterojunction	1–1.4 μm	90%	τ_R = 120 ps	[117]
$Ga_{0.58}Al_{0.42}As_{0.02}Sb_{0.98}/Ga_{0.84}Al_{0.16}Sb/GaSb$	p^+-n-n^+ heterojunction	1–1.4 μm	90%	τ_R = 120 ps	[118]
$Ga_{0.76}Al_{0.24}As_{0.023}Sb_{0.977}/Ga_{0.8}Al_{0.2}As_{0.019}Sb_{0.981}/GaSb/$ $/GaSb$ (mesa, LPE)	n^+-p-p-p^+ homo- and heterojunctions	1.25–1.35 μm	90%	τ_R = 120 ps	[118]

An etched, inverted mesa-type GaInAsP/InP avalanche diode, in which a similar separation of the generation and multiplication regions is achieved by means of a grown InP *p-n* junction, has recently been made [122] and found to have extra-low dark current and excellent noise characteristics.

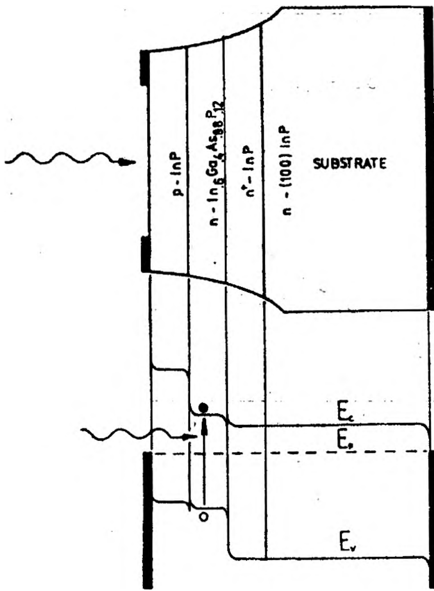

Fig. 6. The III–V quaternary detector prepared in mesa configuration, from [41] (above), and its energy-band diagram (below)

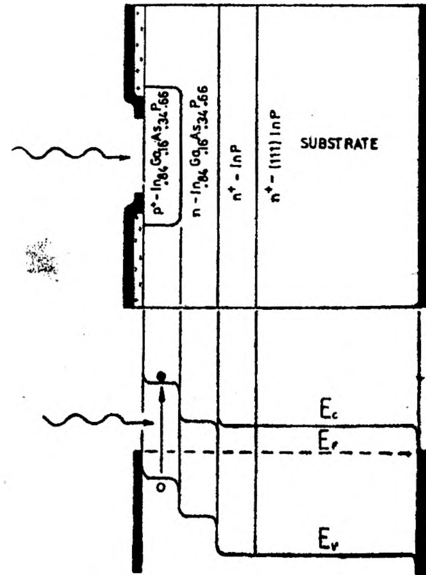

Fig. 7. The III–V quaternary detector prepared in planar configuration, from [42] (above), and its energy-band diagram (below)

Some attempts were also made to obtain the near-infrared fiber-optic detectors from materials other than the mentioned above; for example, the $MnSb_2S_4$ single crystal exhibits 1-eV-energy gap [43] and amorphous p^+-$Se_{0.95}Te_{0.05}$/p-$Se_{0.7}Te_{0.3}$ heterostructure operates as a photovoltaic detector in 1.0–3.5 μm wavelength range [44].

5. The proposal of a graded-gap fiber-optic detector

As it was already mentioned in the previous Chapter, a detector made of (Al, In) Sb, Ga(As, Sb) or In(P, As) for the 1.2–1.3 μm-wavelength range has not been prepared yet. Since gallium arsenide substrates are still the most readily available, the only alloy mentioned above, that can be grown on this substrate is the Ga(As, Sb) mixed crystal.

Figure 8 shows the composition-dependent energy gap of $GaAs_{1-x}Sb_x$. This alloy exhibits an appropriate energy gap for $x = 0.27$, which is derived

from the composition-dependent energy-gap equation for $GaAs_{1-x}Sb_x$ [45]

$$E_g(300\ \mathrm{K}) = 1.43-1.9x+1.2x^2,\ (\mathrm{eV}). \tag{10}$$

Figure 9 shows the dependence of $GaAs_{1-x}Sb_x$ lattice constant upon composition, according to Vegard's law [46]. It is easily seen that for two extreme

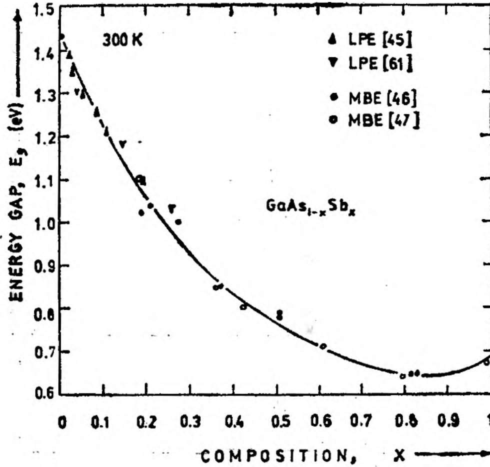

Fig. 8. Compositional dependence of the $GaAs_{1-x}Sb_x$ mixed-crystal energy gap, from [45, 47, 56, 61]

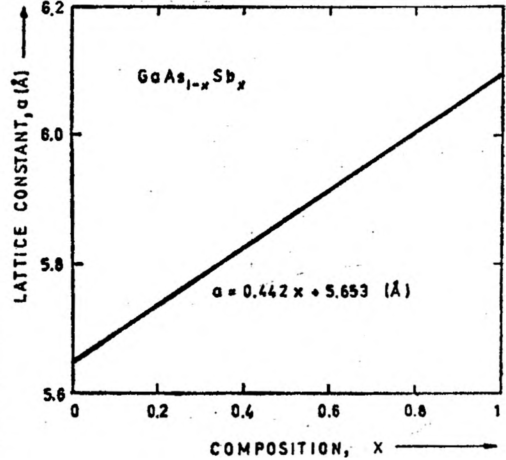

Fig. 9. Compositional dependence of the $GaAs_{1-x}Sb$ mixed-crystal lattice constant, from [46]

compositions: $x = 0$ and $x = 1$ the lattice mismatch equals almost 8%. According to YANO et al. [47] this lattice mismatch will cause an inhomogeneous distribution of defects near and within the substrate-epilayer interface, within which the space-charge region is formed. This effect influences the mobility of the current carriers. NAHORY et al. [45] have determined the boundary GaSb mole fraction, above which epilayers cannot be readily grown directly on GaAs substrates without gross macroscopic defects. This fraction equals 0.17. The authors of [45] have also pointed out that liquid-phase epitaxial (LPE) technique involves unintentional compositional grading due to the growth on non-lattice-mathed GaAs substrates. CHANG et al. [48]. who applied molecular-beam epitaxial (MBE) technique, noticed that when the mismatch was smaller than 2.5% the growth proceeded smoothly and without interruption. SAKAI et al. [46], who also applied the MBE technique, c ontrolled the composition as to achieve a lattice match to within about 2.5%. In consequence, he obtained planar and abrupt junctions, with compositional grading less than a few angstroms. YANO et al. [47], who deposited also GaSb single crystal on GaAs substrates by molecular-beam epitaxy, suggested that a h'gher quality epitaxial layer would be obtained by applying compositional grading or GaSb substrate. In order to relieve the strain of lattice mismatch between the substrate and the grown junction PEARSALL et al. [49] used the intermediate layers. Ga(As, Sb) photodiode with energy gap corresponding to 1.06 μm was prepared

on GaAs substrate by LPE method. Another way of reducing the strain due to the lattice mismatch is to deposite a relatively thick first layer of Ga(As, Sb). This was done by SUGIYAMA et al. [50] in the form of an over 20 μm thick linking epilayer.

It goes without saying that due to the application of an extra compositionally-graded layer better detectors parameters could be achieved and all heterojunction disadvantages in the active area avoided. The band diagram of such a detector is shown in Fig. 10. If the employed GaAs substrate is of n-type, the grown epilayer is of p-type; then a p-n junction may be unintentionally obtained.

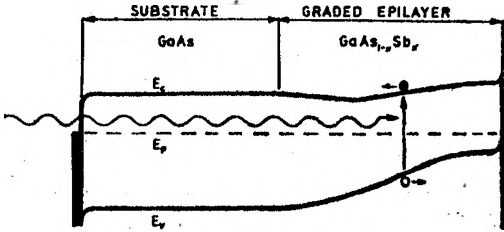

Fig. 10. Energy-band diagram of the compositionally graded bandgap $GaAs_{1-x}Sb$ mixed-crystal photovoltaic detector

Undoped layers of $GaAs_{1-x}Sb_x$ were found by NAHORY et al. [45] to be n-type with electron concentration of about 10^{16} cm^{-3} for composition x no greater than 0.14. According to the authors' [45] prediction for the values of x closer to unity the undoped material would behave more like GaSb being normally p-type as-grown. GaSb single crystals grown from a melt [51, 52] as well as grown by the MBE technique [47] usually have hole concentration of about 10^{17} cm^{-3} and the holes presumably come from excess Ga on an Sb sublattice site. CHANG et al. [48] have found out that undoped GaSb is p-type with a carrier mobility of 670 m^2 V^{-1} s^{-1}. According to the authors [48], $GaAs_{1-x}Sb_x$ films remained of p-type for x ranging at least from 0.3 to 1. The carrier concentration in these undoped films was found to be 5×10^{16} cm^{-3}. BRIERLEY et al. [53] used the Si amphoteric dopant, among others, to reduce the formation of p-n junction during the growth of a $GaAs_{1-x}Sb_x$ single layer. This fact confirms the posibility of unintentional formation of a p-n junction during the growth process. If, however, the substrate is doped to a high level of dopant concentration, these dopants are able to diffuse from the substrate to the grown epilayer and when it is thin enough, to compensate it. In this case the doping process ought to be such as to secure the formation of p-n junction far from the interface between the grown layer and the substrate.

6. Epitaxial growth of $GaAs_{1-x}Sb_x$

The purpose of this Chapter is to give a brief outline of different so far developed epitaxial techniques for growing Ga(As, Sb), the list of suitable references, and to present a proposal concerning the use of liquid-phase electroepitaxy to grow high-quality Ga (As, Sb) layers.

6.1. Vapour-phase epitaxy (VPE)

The first widely known successful attempt in growing single crystals of $GaAs_{1-x}Sb_x$ ternary alloys was made by DAY [54] with the help of VPE method. Antimony pentachloride was used as a source of antimony vapour. The limitation of this method consisted in condensation of antimony being introduced into the growth zone, resulting in a small antimony content in epitaxially grown layers. The mole fraction x in the layers was less than about $2^0/_0$ and the author did not succeed in obtaining layers with higher values of x.

CLOUGH et al. [55] used the VPE method to grow $GaAs_{1-x}Sb_x$ with x ranging from 0.01 to 0.08. They were the first published results of preparation for this compositional range. There antimony pentachloride was replaced by stibine, the arsenic and antimony hydrides, i.e., arsine (AsH_3) and stibine (SbH_3) were used as sources of the group V elements. The authors had to face the problems with stibine decomposition taking place immediately after heating. To delay the decomposition high flow velocities were employed. This enabled the stibine to reach the reaction zone without being condensed in the system in form of antimony. It has been pointed out that low growth rates due to low melting point of gallium antimonide (712 °C) and the low vapour pressure of antimony at that temperature (less than 1 Torr) were the main limitations of the method used. In order to improve the growth rates of the GaSb-rich ternary alloys, the growth temperature was maintained just below the alloy solidus since then the partial pressure of antimony in the system could reach the maximum. However, due to the thermodynamic limitations mentioned above, the growth rates did not exceed 5 μm/h. The diagram of the vapour deposition apparatus used in [55] is shown in Fig. 11. HCl was introduced over the gallium

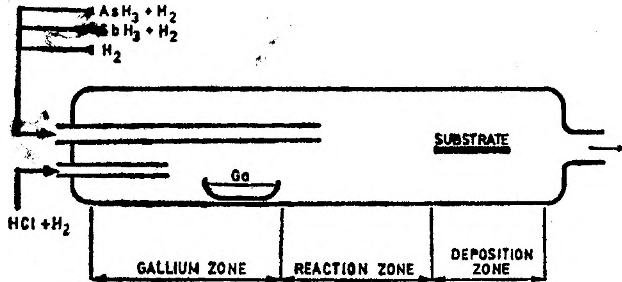

Fig. 11. Schematic diagram of the VPE deposition set-up for growing $GaAs_{1-x}Sb_x$, from [55]

boat maintained at 850 °C to transport the gallium, mainly in form of subchloride, to the reaction zone kept at the same temperature, where the latter reacted with arsenic and antimony, and was deposited on the substrate surface maintained at temperature ranging from 650 to 750 °C. The substrates were single-crystal semi-insulating GaAs oriented 3 deg off the (100) axis. The decomposition of the grown epilayers was independent of the growth temperature, being dependent only upon the mole fraction of antimony in the vapour phase that was always greater than that obtained in the epilayer. The grown layers

had relatively low Hall coefficients. This effect was explained by the lattice mismatch and the difference in thermal expansion coefficients between the substrate and the epilayer. The authors suggested that higher mobilities might be expected by employing a compositional grading.

MANASEVIT et al. [56] grew Ga(As, Sb) with organometallic vapour-phase epitaxy (OM VPE) using trimethylogallium arsine and stibine, the latter being difficult to handle and being replaced by trimethylantimony. The process was carried out at temperature of 725 °C and the compounds were deposited on (100) GaAs and (0001) Al_2O_3. Better parameters of the grown layers were achieved when deposited on GaAs substrate. The composition x ranged from 0.1 to 0.3 and was controlled by keeping constant the ratio of the arsenic flow to the antimony flow. The apparatus used is shown schematically in Fig. 12 and consisted of a single vertical quartz tube equipped with an inductive heater of a substrate pedestal.

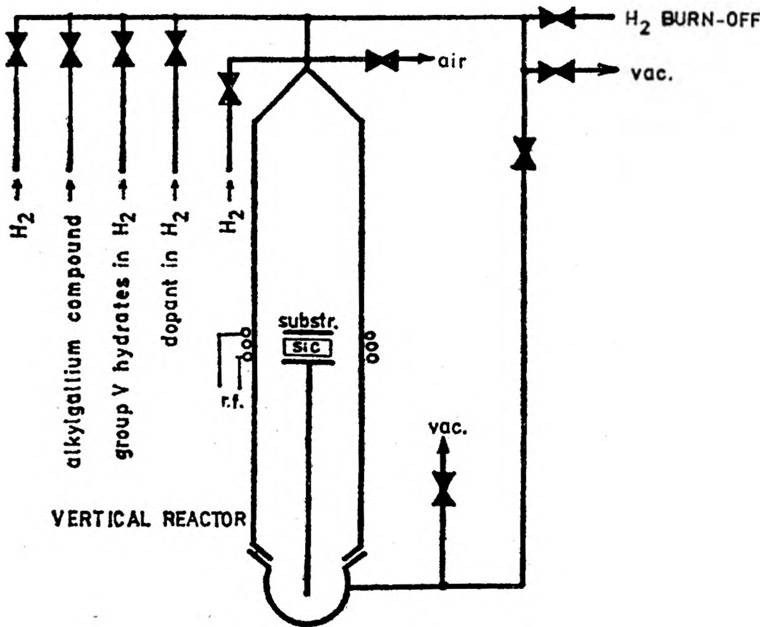

Fig. 12. Schematic diagram of the OMVPE deposition set-up for growing $GaAs_{1-x}Sb_x$, from [56]

COOPER et al. [57] prepared $GaAs_{1-x}Sb_x$ alloys using OM VPE method over the composition range of $0 \leqslant x \leqslant 0.11$. The authors demonstrated that the column V trialkyls (trimethylantimony and trimethylarsenic) had particular advantages in some cases over the column V trihydrides. As a source of gallium, trimethylgallium was used. In the case of Ga(As, Sb), the OM VPE method, allowing to obtain higher antimony concentrations in the gase phase and higher growth rates and more uniform growths, appeared to be superior to that of the HCl-transport VPE. Growths were performed at temperatures ranging from 500 to 630°C using a trimethylgallium:trihydride arsine:trimethylantimony mole fraction ratio of 2.4 : 1 : 2.4. Above the growth temperature of 625 °C

very high Sb concentrations were not attainable. Thus, in the OM VPE method the solid composition is growth temperature dependent opposite to the HCl-transport VPE.

6.2. Liquid-phase epitaxy (LPE)

The LPE technique used in preparing $GaAs_{1-x}Sb_x$ has been reported by few researches. First successful attempts were made at the very beginning of the seventies. A considerable concentration difference between the solidus and liquidus curves in the pseudobinary phase diagram of GaAs-GaSb system (as illustrated in Fig. 13) may involve certain difficulties in the application of LPE

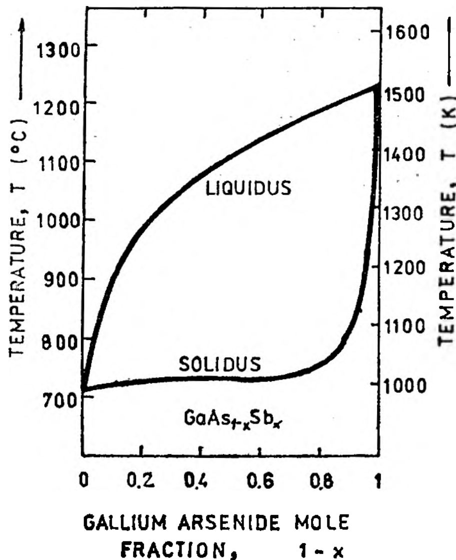

Fig. 13. Pseudobinary phase diagram of the GaAs-GaSb system, from [45, 61]

technique to this system. Another limitation of using this method is a possible existence of a miscibility gap, which is believed to be no larger than a certain composition range that varies from paper to paper [45, 58–60].

ANTYPAS et al. [61] used the technique basing on the LPE of the GaAs homojunction reported by NELSON [62]. The melt was prepared by saturation of Ga metal with As from a GaAs source at the starting growth temperature of 720°C. The GaAs addition to the melt involved the formation of Ga(As, Sb) dendrities being in equilibrium with the melt. Zinc was udes as a dopant. The oven was tilted approximately 10° from the horizontal position to make the melt roll over the Cr-doped (100) GaAs substrate. At the end of the cooling cycle ($\Delta T = 37.5$°C) the oven was tipped to the horizontal position. This technique was used to achieve compositions $x \leqslant 0.25$. The grown sample was used for production of a high-efficiency long-wavelength threshold photoemitter [61].

Precisely the same technique was used by ANTYPAS et al. in [63], in preparing the semitransparent photocathode made of $GaAs_{1-x}Sb_x$. The 5 μm thick

layer of $GaAs_{0.95}Sb_{0.05}$ was prepared with the lattice mismatch between the substrate and the epitaxial layer equal to $0.39^0/_0$, and an 8 μm thick layer of $GaAs_{0.83}Sb_{0.17}$ with the mismatch of $1.4^0/_0$. The authors observed that for a lattice mismatch of less than $0.75^0/_0$ the obtained layers were free from any grain boundaries. For mismatches greater than that, the density of the grain boundaries increased monothonically with the lattice mismatch.

SUGIYAMA et al. [50] prepared the $GaAs_{1-x}Sb_x$ alloy and quaternary (Al, Ga) (As, Sb) alloy from the Ga solution on *n*-type (100) GaAs substrates in purified hydrogen atmosphere. Both *n*- and *p*-types $GaAs_{1-x}Sb_x$ were grown with Sn and Si as dopants, respectively. To reduce the effect of the lattice mismatch the deposited layer of $GaAs_{1-x}Sb_x$ was relatively thick (20–30 μm). The composition of the grown layers was estimated to be approximately $x = 0.15$. The grown material was used for preparation of the double heterojunction laser.

ANTYPAS et al. [64] made lattice-matched heterojunctions of $GaAs_{1-x}Sb_x/$ $/Al_yGa_{1-y}As_{1-v}Sb_v$. The layers were grown on (100)-oriented GaAs substrates, in a horizontal growth system using a palladium purified hydrogen environment and a graphite boat. The initial growth temperatures were 760 ans 720°C. The cooling rate was 1°C/min. over the temperature interval of 20 deg. The epitaxial layers were characterized by electron microprobe, X-ray and photoluminescence measurments to determine the composition of the solid solution, the lattice constant and bandgap thereof. The ternary-solid-solution composition grown in 720–700°C and 760–740°C were $x = 0.065$ and 0.043, respectively, having the corresponding bandgaps of 1.18 and 1.23 eV. The authors pointed out the limitation of the III–V ternary solid solutions that could not be grown directly on III–V binary substrates without introducing lattice-mismatch dislocations at the interface. According to [64], this limitation can be relieved by growing III–V quaternary compounds where lattice matching can be achieved over a wide range of bandgap energy.

BRIERLEY et al. [53] preparated the $GaAs_{1-x}Sb_x$ layers on (100) GaAs substrates by using a horizontal-sliding LPE technique. Silicon was used as both a *p*- and *n*-type dopant (silicon retains its amphoteric behaviour in a Ga(As, Sb) system). The junction was produced by growing the epilayer through the *n*-to-*p* transition temperature. For $GaAs_{0.97}Sb_{0.03}$ and $GaAs_{0.94}Sb_{0.06}$ these temperatures were determined as a function of the atomic percent of silicon in the melt. The authors faced the problem connected with a constitutional supercooling because of a small segregation coefficient of antimony when grown from a gallium-rich melt. The starting growth temperature was fixed at 880°C. Relatively slow cooling rates were used (1.5 °C/min.). The most serious problems were encountered while growing 6% GaSb layers; the growth rate of the above mentioned layer should have been slower than that applied. The grown material was utilized for preparing electroluminescent diodes emitting to 1.06 μm.

PEARSALL et al. [49] prepared an avalanche photodiode made of $GaAs_{1-x}Sb_x$ with the energy gap corresponding to $\lambda = 1.06$ µm. The p-n homojunctions were grown by LPE technique on (100) GaAs Sn-doped substrates. Intermediate layers being used were relatively thick to relieve the strain of the lattice mismatch between the GaAs substrate and the grown junction. Impact ionization rates measured for electrons and holes in $GaAs_{0.95}Sb_{0.05}$, $GaAs_{0.90}Sb_{0.10}$ and $GaAs_{0.88}Sb_{0.12}$ have shown that the ionization rates were strongly affected by material compositions. This effect was particularly important in the design of avalanche photodiodes, where the optimum signal-to-noise performance was obtained when the avalanche gain was initiated by the carrier with a higher ionization coefficient.

NAHORY et al. in [65] produced continuous-operation 1.0 µm wavelength double-heterostructure injection lasers made of $GaAs_{1-x}Sb_x/Al_yGa_{1-y}As_{1-x}Sb_x$ by using a multiple-bin boat and slider assembly.

NAHORY et al. in [45] studied the Ga(As, Sb) ternary phase diagram and both physical and electrical properties of $GaAs_{1-x}Sb_x$ layers over a limited compositional range $0 \leqslant x \leqslant 0.2$. The LPE-reactor consisted of a single-zone horizontally split furnace fitted with additional heater coils to flatten the temperature profile. Palladium-purified hydrogen was flowed through the quartz reaction tube. Starting material for the melt consisted of 99.999 %-pure gallium, 99.99 %-pure antimony and undoped polycrystalline GaAs. Substrates for epitaxial growth were (100)-oriented GaAs wafers. The growth was initiated by bringing the substrate into direct contact with the solution about 2°C below the liquidus temperature which was then cooled at a constant rate through several degrees centigrade. The use of a slightly supersaturated solution facilitated the uniform nucleation of the grown layer. The deviation of the grown layer from the equilibrium solidus composition was found to result from grading due to growth on a non-lattice-matched substrate and constitutional supercooling. In all solutions prepared in [45] arsenic contents were very small being even smaller near the growing layer during the epitaxial growth. The farer the growth proceeded, the more deficient in arsenic, thus the richer in antimony the solid layer was. The change in the solution composition near the epilayer was equivalent to the constitutional supercooling. The calculations showed the possibility of the existence of a miscibility gap depending upon the value of the solidus interaction parameters. The possible miscibility gap was believed to be not wider than $0.55 \leqslant x \leqslant 0.62$. The authors pointed out that epitaxial $GaAs_{1-x}Sb_x$ was not difficult to prepare and that it was of a great interest because of its optoelectronics applications.

CAMPBELL et al. [66] fabricated a burried heterojunction electroabsorption modulator made of the heterostructure of $Al_yGa_{1-y}As_{1-x}Sb_x/GaAs_{1-x}Sb_x$ grown by LPE method on (100)-oriented GaAs wafers. For operation near 1.06 µm, a lattice-matched waveguiding structure was obtained with $x = 0.10$ and $y = 0.25$.

6.3. Molecular-beam epitaxy (MBE)

Although a relatively novel epitaxial growth technique based on molecular beams needs a rather expensive equipment necessary to control the growth process in situ, it provides high-quality epitaxial layers.

WAHO et al. [67] reported $GaAs_{1-x}Sb_x$ growth at a wide composition range, $0.3 < x < 0.9$, by microprocessor-controlled MBE. The growth system used is shown in Fig. 14. Effusion-cell temperatures were regulated during growth

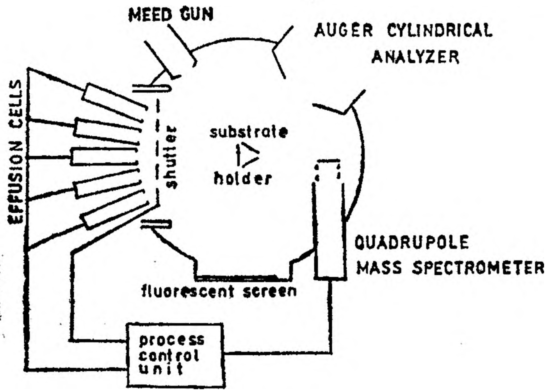

Fig. 14. The MBE growth system for growing $GaAs_{1-x}Sb$, from [67]

by checking quadrupole-mass-spectrometer ion currents or molecular beam intensities. Temperatures of effusion cells for Ga, As and Sb were 900–930°C, 290–330°C, and 540–560°C, respectively. The epilayers grown on Cr-doped semi-insulating (001) GaAs were simultaneously characterized in situ by Auger electron spectroscopy and middle-energy electron diffraction observations. The background pressure just before deposition was of about 10^{-9} Torr, and during growth it increased up to 9×10^{-7} Torr due to arsenic vapour. Growth temperature equaled 550°C throughout the experiment. The epilayers deposited at the rate of about 1 μm/h were 2-3 μm thick, their composition varied smoothly from GaAs to $GaAs_{0.42}Sb_{0.58}$. In conclusion, the authors pointed out that high quality $GaAs_{1-x}Sb_x$ might be expected by using a continuously grading technique.

CHO et al. in [68] chose, among other systems, Ga(As, Sb) layers as being the most suitable for growth due to the following reasons: i) the readily available GaAs substrates can be heated in vacuum to temperature of 630°C, which is high enough to desorb most of the residual surface contaminants [69], ii) layers may be grown at temperatures exceeding 530°C required to prevent the oxygen contamination of the GaAs substrate by the residual water vapour and CO, and iii) phosphorus containing solid solutions cannot be conveniently grown with molecular beam epitaxy at temperatures higher than 450°C because of the required high partial pressure of phosphorus. $GaAs_{1-x}Sb_x$ layers were grown in the way similar to that used for the growth of $Al_xGa_{1-x}As$ solid solutions by CHO et al. in [70]. The background pressure prevailing in the system used in

[68] before liquid-nitrogen trapping was 5×10^{-8} Torr and during the growth it rose to 10^{-6} Torr due to untrapped arsenic. The n-type $GaAs_{0.9}Sb_{0.1}$ layer was grown on a 6 μm thick compositionally graded region grown on a GaAs semi-insulating substrate. Continuous grading was achieved by varying the temperature of the Sb effusion cell from 300 to 460°C. The temperatures of the Ga-, As-, and Sn-effusion cells were kept at 980°C, 350°, and 800°C, respectively. The substrate was kept at 580°C during the growth process. The GaAs mole fraction was estimated from the photoluminescence peak intensity [61, 68].

SAKAI et al. [46] prepared $GaAs_{1-x}Sb_x$ layers in order to investigate the transport properties in $In_xGa_{1-x}As/GaAs_{1-x}Sb_x$ heterojunctions. The MBE system was that used previously for growth of other III–V compounds [71]. According to [46] the MBE was chosen for preparation of the heterojunctions because it gave the possibility to achieve smooth and abrupt interfaces with the compositional grading less than a few angstroms when the interface lattice mismatch was kept within about 2.5%. About 2 μm thick films of $GaAs_{1-x}Sb_x$ ($x > 0.3$) were grown at the rate of 0.1–0.3 nm/s after deposition of a homoepitaxial film of about 100 nm on p-type (100) GaSb substrates. The epilayers of $GaAs_{1-x}Sb_x$ being undoped were mostly p-type with hole concentration of about 5×10^{16} cm^{-3}. The growth was monitored by high-energy-electron diffraction, X-ray diffraction with Auger electron spectroscopy being employed to check the compositions in situ.

CHANG et al. [48], using previously mentioned method [46], prepared $GaAs_{1-x}Sb_x$ films over the whole composition ranges on (100) GaAs and GaSb substrates. In order to smooth the substrate surface out, a 100 nm thick buffer homoepitaxial layer was deposited prior to ternary alloy growth. Results obtained for both GaAs and GaSb substrates showed no noticeable difference The deposition was carried out at the temperature of 450–600°C and the growth rate was 0.1–0.3 nm/s. The composition of the grown layers was measured in situ by Auger electron spectroscopy and deposition monitored in situ by reflection high-energy electron diffraction. The compositions of the films were checked with X-ray diffraction and electron-microprobe analyses. The compositions measured were found to be within 5%. In order to investigate the lattice-mismatch impact on the epilayer structure, the $GaAs_{0.20}Sb_{0.8}$ layer was grown on GaAs substrate for which the lattice mismatch amounted to 6.2%. The authors found out that the growth proceeded smoothly when the mismatch was smaller than about 2.5%. Otherwise the three-dimensional nucleation step intervened at the initial stage of heteroepitaxial growth. The $GaAs_{1-x}Sb_x$ growth rate was governed by the Ga arrival rate, while the ternary alloy composition was determined by the competition between the Sb and the As, where the Sb was playing the dominant role. The dominance of Sb incorporation over that of As was found to be consistent with the thermodynamic properties of Sb_4 and As_4 [72]. It decreased with the increasing substrate temperature. The authors did not find any miscibility gap suggesting that its existence might depend significantly upon the growth technique used. Also electrical properties of the obtained

layers were examined. Undoped GaSb was found to be p-type material with a carrier mobility of 670 cm²/Vs and undoped $GaAs_{1-x}Sb_x$ remained p-type within the range of $0.3 \leqslant x \leqslant 1$. Sn revealed its amphoteric behaviour as a dopant. The dopant used made the alloy p-type for $x \gtrsim 0.86$ and n-type for $x \lesssim 0.82$. The authors observed also the correlation between the dopant behaviour and the surface reconstruction pattern.

YANO et al. [47] prepared GaAs and $GaAs_{1-x}Sb_x$ in the experimental apparatus containing three cylindrical effusion cells for Ga, As and Sb, and similar to that used for growing other III–V compounds [73]. The temperatures of the cells were 1050°, 550–650°C, and 290–350°C for Ga, Sb and As, respectively. The epilayers were characterized and evaluated with a scanning electron microscope, refractive high-energy electron diffraction, X-ray diffraction, ion microprobe analyzer and electrical measuerments. $GaAs_{1-x}Sb_x$ epilayers of the entire composition were grown on (100)-oriented, Cr-doped semi-insulating GaAs wafers at the temperature of 530°C thorought the deposition. The obtained layers showed high crystallinity and in-depth uniformity of the composition. The native defects situated within the graded layer were found as being formed unintentionally and thin compared with the whole film thickness. The authors suggested that the higher quality epitaxial layer might be obtained by using intentionally compositional grading to avoid the defects at the interface.

6.4. Liquid-phase electroepitaxy (LPEE)

So far no description of the preparation of $GaAs_{1-x}Sb_x$ by the LPEE growth techniques has been reported.

The fundamental principle of the technique is shown in Fig. 15. The technique developed a few years ago [74, 75] consists in the current-induced growth, the temperature of the system being maintained constant. Due to the electric current flow in the appropriate direction both the solute electromigration and Peltier cooling lead to supersaturation at the substrate-solution interface which,

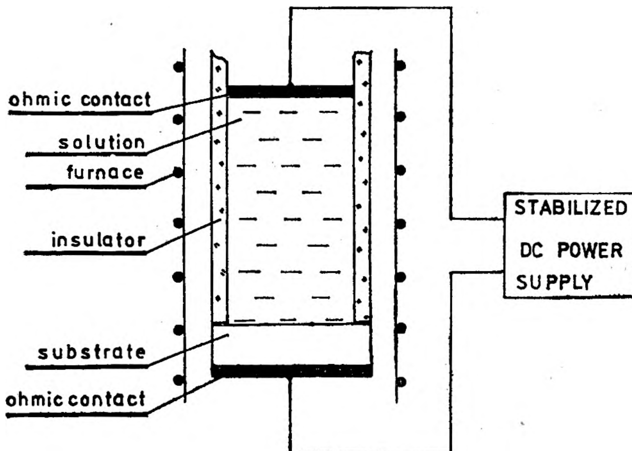

Fig. 15. Illustration of the fundamental principle of the liquid-phase electroepitaxial growth, from [74]

in turn, leads to crystal growth. The electric current plays the most important role in the interface temperature and solute transport control. Much has been done on electroepitaxy [74–95], to this end electroepitaxially grown multicomponent III–V systems, e.g., $Al_xGa_{1-x}As$ [76, 78, 87, 94] have been prepared. The layers of these systems, grown with LPEE, showed the parameters far more superior to those grown with standard LPE. Therefore, it is expected that the application of the LPEE technique to the Ga(As, Sb) system might improve the obtained layers.

7. Final remarks

A brief presentation of recently published results given above shows the great advantage of mixed ternary and quaternary III–V compound semiconductors over all known materials, especially as far as a low level of the dark current and low excess noise factor are concerned. The avalanche diodes in which the separation of the generation and multiplication regions is done by advanced preparation methods have recently been produced [122] and found to have the extra-low dark current and excellent noise characteristics.

The proposed graded-gap Ga(As, Sb) fiber-optic detector combines the mentioned above and the additional advantages: i) the graded-gap-window structure protects the diffusion of excess carriers towards the surface with higher recombination rates, due to the existence of additional internal quasi-electric fields acting on carriers [13], and ii) due to compositionally graded layer all heterojunctions disadvantages in the active area can be avoided. The experimental work on graded-gap Ga(As, Sb) detector is currently performed by the authors.

Acknowledgements – The authors express their best thanks to Professor B. Paszkowski for his interest in this work. The financial support of the Polish Academy of Sciences is gratefully acknowledged.

References

[1] KIMURA, T. IEEE Trans. CAS-**26** (9179), 987.
[2] HURWITZ, C. E. Optical Engineering **20** (1981), 658.
[3] YAMAMOTO, T. SAKAI K., AKIBA S., SUEMATSU Y., IEEE Trans. **QE-14** (1978), 95.
[4] MAHAJAN S., JOHNSTON W. D. Jr., POLLOCK M. A., NAHORY R. E., Appl. Phys. Lett. **34** (1979), 717.
[5] KANO H., OE K., ANDO S., SUGIYAMA K., Jap. J. Appl. Phys. **18** (1979), 2333.
[6] KIMURA T., DAIKOKU K., Opt. Quantum Electron. **9** (1977), 33.
[7] MIYA T., TERENUMA Y., HOSAKA T., MIYASHITA T., Electron. Lett. **15** (1979), 108.
[8] KEYES R. J., *Optical and Infrared Detectors,* Topics in Applied Physics, Vol. 19, Springer-Verlag, Berlin 1977.
[9] LONG D., IR Phys. **7** (1967), 121.
[10] PENCHINA C. M., IR Phys. **15** (1975), 9.
[11] TAUC J., Rev. Modern Phys. **29** (1957), 308.

[12] KRUSE P. W., Appl. Opt. **4** (1965), 687.
[13] PAWLIKOWSKI J. M., IR Phys. **20** (1978), 257.
[14] MCINTYRE R. J., IEEE Trans. **ED-13** (1966), 164.
[15] PUTLEY E. H., Appl. Opt. **4** (1965), 649.
[16] KIMMITT M. F., IR Phys. **17** (1977), 459.
[17] MOSS T. S., BARRELL G. J., ELLIS B., *Semiconductor Optoelectronics,* Butterworth, London 1973.
[18] STILLMAN G. E., WOLFE C. M., ROSSI J. A., RYAN J. L., Proc. Symp. Opt. Acoust. Microelectron., New York 1974, Polytech. Press, Brooklyn, New York 1975, p. 543.
[19] JOHSTON W. D. Jr., CALLAHAN W. N., Proc. Int. Electron Devices Meeting, Washington 1976, IEEE (1976) p. 461.
[20] SERAFETINIDES A. A., KAR A. K., KIMMITT M. F., Opt. Laser Technol. **10** (1978), 243.
[21] LEBEDEV A. A., AKHMEDOV F. A., AKHMEDOVA M. M., Sov. Phys. Semicond. **10** (1976), 1029.
[22] PROTSCHKA H., SHANG D. C., Int. Electron Devices Meeting, Washington, D. C., 1967.
[23] MOSS T. S., IR Phys. **16** (1976), 95.
[24] SODERMAN D. A., PINKSTEN W. H., Appl. Opt. **11** (1972), 2161.
[25] FIORITTO G., GASPARINI G., SVELTO F., IR Phys. **18** (1978), 59.
[26] BECLA P., PAWLIKOWSKI J. M., IR Phys. **16** (1976), 457.
[27] PAWLIKOWSKI J. M., Thin Solid Films **50** (1978), 269.
[28] BOISSY M. C., DIGENT D., HALLAIS J., SCHEMALI C., Proc. 6th Int. GaAs and Related Compounds, Edinburgh 1976, Inst, Phys., London 1977, Part I, p. 427.
[29] PEARSALL T. P., DUDA E., PAPUCHON M., ROULLET E., Topical Meeting on Integrated and Guided Wave Optics, Salt Lake City 1977, Opt. Soc. Am. (1977), p. MC2/1–3.
[30] PEARSALL T. P., NAHORY R. E., POLLOCK M. A., Appl. Phys. Letts. **27** (1975), 330.
[31] ENSTROM R. E., RICHMAN D., ABRAHAMS N. S., APPERT I. E., FISCHER D. G., SOMMER A. H., WILLIAM B. F., Proc. 3rd Int. Symp. on GaAs and Related Compounds. Inst. Phys., London 1971, p. 30.
[32] SANKARAN R., MOON R. L., ANTYPAS G., J. Cryst. Growth **33** (1976), 271.
[33] ANDO H., KANBE H., ITO M., KANEDA T., Jap. J. Appl. Phys. **19** (1980), L277.
[34] SUSA N., YAMAUCHI Y., ANDO H., KANBE H., Jap. J. Appl. Phys. **19** (1980), L17.
[35] CHENG K. V., PEARSON G. L., J. Electrochem. Soc. **124** (1977), 753.
[36] ANDERSON S. J., SCHOLL F., HARRIS J. S., in Ref. [28], Part II, p. 346.
[37] LAW H. D. TOMASETTA L. R., NAKANO K., HARRIS J. S., Appl. Phys. Lett. **33** (1978), 416.
[38] HURWITZ C. E., HSIEH J. J., WALPOLE J. N., S. H. GROVES, Proc. Conf. "Eascon '78", Arlington, VA., 1978, IEEE, (1978), p. 496.
[39] TAKANASHI Y., HORIKOSHI Y., Jap. J. Appl. Phys. **19** (1980), L163.
[40] LAW H. D., NAKANO K., TOMASSETTA L. R., IEEE Trans. **QE-15** (1979), 549.
[41] WASHINGTON M. A., NAHORY R. E., POLLOCK M. A., BEEBE E. D., Appl. Phys. Lett. **33** (1978), 854.
[42] LAW H. D., TOMASSETTA L. R., NAKANO K., Appl. Phys. Lett. **33** (1978), 920.
[43] RUSTAMOV P. G., GUSEINOVA M. A., ALIDZANOV M. A., SAHAROV M. G., Inorg. Mater. **12** (1976), 1482 (in Russian).
[44] KIKUCHI T., EMA Y., HAYASHI T., J. Appl. Phys. **50** (1979), 5043.
[45] NAHORY R. E., POLLOCK M. A., DEWINTER J. C., WILLIAMS K. M., J. Appl. Phys. **48** (1977), 1607.
[46] SAKAI H., CHANG L. L., JUDEKE R., CHANG C. A., SAI-HALASH G. A., ESAKI L., Appl. Phys. Lett. **31** (1977), 211.
[47] YANO M., SUZUKI Y., ISHII T., MATSUSHIMA Y., KIMATA M., Jap. J. Appl. Phys. **17** (1978), 2091.
[48] CHANG C., LUDEKE R., CHANG L. L., ESAKI L., Appl. Phys. Lett. **31** (1977), 759.
[49] PEARSALL T. P., NAHORY R. E., POLLOCK M. A., Appl. Phys. Lett. **28** (1976), 403.

[50] SUGIYAMA K., SAITO H., Jap. J. Appl. Phys. **11** (1972), 1057.
[51] EFFER D. ETTER P. J., J. Phys. Chem. Solids **25** (1965), 451.
[52] BAXTER R. D., BATE R. T., REID F. J., J. Phys. Chem. Solids **26** (1965), 41.
[53] BRIERLEY S. K., FONSTAD C. G., J. Appl. Phys. **46** (1975), 3678.
[54] DAY G. F., *New Gunn Fffect Materials*, Varian Assoc. Technical Report AFAL-TR-67-2, March 1972 (unpublished).
[55] CLOUGH R. B., TIETJEN J. J., Trans. Met. Soc. AIME, **245** (1969), 583.
[56] MANASEVIT H. M., SIMPSON W. I., J. Electrochem. Soc. **116** (1969), 1725.
[57] COOPER C. B., LUDOWIZE M. J., AEBI V., MOON R. L., J. Electron, Mater. **9** (1980), 299.
[58] FOSTER L. M., J. Electrochem. Soc. **121** (1974), 1662.
[59] GRALTON M. F., WOOLLEY J. C., J. Electron Mater. **2** (1973), 455.
[60] STRAUMANIS M. E., KIM C. D., J. Electrochem. Soc. **112** (1965), 112.
[61] ANTYPAS G. A., JAMES L. W., J. Appl. Phys. **41** (1970), 2165.
[62] NELSON H., RCA Rev. **24** (1963), 603.
[63] ANTYPAS G. A., JAMES L. W., UEBBING J. J., J. Appl. Phys. **41** (1970), 2888.
[64] ANTYPAS G. A., MOON R. L., J. Electrochem. Soc. **121** (1974), 416.
[65] NAHORY R. E., POLLOCK M. A., BEEBE E. D., DEWINTER J. C., Appl. Phys. Lett. **28** (1976), 19.
[66] CAMPBELL J. C., DEWINTER J. C., POLLOCK M. A., NAHORY R. E., Appl. Phys. Lett. **32** (1978), 471.
[67] WAHO I., OGAWA S., MARUYAMA S., Jap. J. Appl. Phys. **16** (1977), 1875.
[68] CHO A. Y., CASEY H. C. Jr., FOY P. W., Appl. Phys. Letts **30** (1977), 397.
[69] CHO A. Y., [in] *Progress in Solid State Chemistry*, ed. by J. O. McCaldin, G. Somorjai, Pergamon, New York 1975, Vol. 10 p. 157.
[70] CHO A. Y., Appl. Phys. Lett. **28** (1976), 501.
[71] CHANG L. L., ESABI L., HOWARD W. E., LUDEKE R., SCHULL G., J. Vac. Sci. Technol. (1973), 655.
[72] HULGREN R., DEASAI P. D., HAWKINS D. T., GLEISER D. T., GLEISER M., KELLEY K. K. WAGMAN D. D., *Selected Values of the Thermodynamics Properites of the Elements*, Metals Park, Ohio 1973.
[73] YANO M., NOGAMI M., MATSUSHIMA Y., KIMATA M., Jap. J. Appl. Phys. **16** (1977), 2131.
[74] KUMAGOWA M., WITT A. F., LICHTENSTEIGER M., GATOS H. C., J. Electrochem. Soc. **120** (1973), 583.
[75] GATOS H. C., JASTRZEBSKI L., USA Patent No. 4, 186, 045, 1980.
[76] DANIELE J. J., MICHEL C., Proc. Int. Symp., GaAs and Related Compounds, Deauville 1974, Inst. Phys. Conf. Series, **24** (1975), 155.
[77] LAWRENCE D. J., EASTMAN L. F., J. Cryst. Growth, **30** (1975), 267.
[78] DANIELE J. J., Appl. Phys. Lett. **27** (1975) 373.
[79] STEFANOKOS E. K., ABUL-FADL A., WORKMAN M. D., J. Appl. Phys. **46** (1975), 3002.
[80] BLOM G. M., DANIELE J. J., KYROS T., WITT A. F., J. Electrochem. Soc. **122** (1975), 1541.
[81] JASTRZEBSKI L., GATOS H. C., Proc. Int. Conf. GaAs and Related Compunds, St. Louis 1976, Inst. Phys. Conf. Ser., Vol. 336, p. 88.
[82] JASTRZEBSKI L., GATOS H. C., WITT A. F., J. Electrochem. Soc. **129** (1976), 1121.
[83] ABUL-FADL A., STEHANOKOS E. K., J. Appl. Phys. **37** (1976), 4627.
[84] LAWRENCE D. J., EASTMAN L. F., J. Electron. Mater. **6** (1977), 1.
[85] ABUL-FADL A., STEHANOKOS E. K., J. Cryst. Growth **90** (1977), 341.
[86] JASTRZEBSKI L., GATOS H. C., J. Cryst. Growth **42** (1977), 341.
[87] DANIELE J. J., CAMMACK D. A., ASBECK P. M., J. Appl. Phys. **48** (1977), 914.
[88] DANIELE J. J., J. Electrochem. Soc. **124** (1977), 1143.
[89] BRYSKIEWICZ T., J. Cryst. Growth **43** (1978), 567.
[90] JASTRZEBSKI L., LAGOWSKI J., GATOS H. C., WITT A. F., J. Appl. Phys. **49** (1978), 5909.

[91] JASTRZEBSKI L., IMAMURA Y., GATOS H. C., J. Electrochem. Soc. **125** (1978), 1140.
[92] IMAMURA Y., JASTRZEBSKI L., GATOS H. C., J. Electrochem. Soc. **125** (1978), 1560.
[93] LAGOWSKI J., JASTRZEBSKI L., GATOS H. C., I. Appl. Phys. **51** (1980), 364.
[94] BRYSKIEWICZ T., LAGOWSKI J., GATOS H. C., J. Appl. Phys. **51** (1980), 988.
[95] BRYSKIEWICZ T., [in] *Semiconductor Optoelectronics*, ed. M. A. Herman, Proc. 2nd Int. School, Cetniewo 1978. PWN, Warsaw 1980, p. 187.
[96] FEUCHT D. L., J. Vacuum Sci. and Technol. **14** (1977), 57.
[97] THOMAS M. B., CODERRE W. M., WOOLLEY J. C., Phys. Stat. Sol. a**2** (1970), K141.
[98] THOMPSON A. G., WOOLLEY J. C., Can. J. Phys. **45** (1967), 255.
[99] LOOK D. C., J. Appl. Phys. **49** (1978), 3543.
[100] NICHOLS K. H., CHANG W. S. C., WOLFE C. M., STILLMAN G. E., Appl. Phys. Letts **31** (1977), 631.
[101] LUCOVSKY G., LASSER M. E., EMMONS RF. B., Proc. IEEE **51** (1963), 166.
[102] PAGEL B. R., PETRITZ R. L., J. Appl. Phys. **31** (1961), 1901.
[103] MELCHIOR H., LYNCH W. T., IEEE Trans. ED-**13** (1966), 829.
[104] MATHUR D. P., MCINTYRE R. J., WEBB P. P., Intern. Electron. Devices Meeting, Washington, D. C., 1968.
[105] KANEDA T., IEEE Trans. **QE-14** (1978), 804.
[106] BARNES C. E., J. Appl. Phys. **50** (1979), 5242.
[107] AHMAD K., MABBITT A. W., Solid State Electron. **22** (1979), 327.
[108] BACHMAN K. J., SHAY J. L., Appl. Phys. Lett. **33** (1978), 446.
[109] PEARSALL T. P., PAPUCHON M., Appl. Phys. Lett. **33** (1978), 640.
[110] SUKEGAWA T., HARAGUCHI T., TANAKA A., HAGINO M., Appl. Phys. Lett. **92** (178), 376.
[111] CLAWSON A. R., LUM W. Y., WIEDER H. H., Proc. of SPIE Conference, Vol. 132, 1978, p. 346.
[112] CLAWSON A. R., LUM W. Y., WIEDER H. H., Opt. Engin. **17** (1978), 666.
[113] LEE T. P., BURRUS C. A., DENTAI A. G., IEEE Trans. **QE-15** (1979), 30.
[114] LEE T. P., BURRUS C. A., DENTAI A. G., BALLMAN A. A., BONNER W. A., Appl. Phys. Lett. **35** (1979), 511.
[115] BURRUS C. A., DENTAI A. G., LEE T. P., Electron. Lett. **15** (1979), 655.
[116] HURWITZ C. E., HSIEH J. J., Appl. Phys. Lett. **32** (1978), 487.
[117] TOMASSETTA L. R., LAW H. D., EDEN R. C., DEYHIMY I., NAKANO K., IEEE Trans. **QE-14** (1978), 800.
[118] TOMASETTA L. R., LAW H. D., NAKANO K., Laser Focus **14** (1978), 42, 44.
[119] BRAIN M. C., Electron. Lett. **15** (1979), 821.
[120] KANEDA T., KAGAWA S., MIKAWA T., TOYAMA Y., Appl. Phys. Lett. **36** (1980), 572.
[121] ANDO H., KANBE H., KIMURA T., YAMAOKA T., KANEDA T., IEEE Trans. **QE-14** (1978), 804.
[122] DIADIUK V., GROVES S. H., HURVITZ C. E., Appl. Phys. Lett. **87** (1980), 807.

Received December 9, 1981
in revised form September 22, 1982

Волокнистые детекторы

Произведён краткий обзор волокнистых детекторов с учётом конструктивных параметров для $\lambda = 1.3$ мкм. Кратко обсуждены экспериментальные данные таких детекторов, содержащие технологические данные, методы действия, а также основные параметры детектора. Приведён обзор свойств полупроводников, использованных в волокнистых системах передачи. Особое внимание уделено свойствам, а также технологии соединений типа Ga (As, Sb). В конечной части предложен детектор, выполненный из смешанного кристалла типа Ga (As, Sb) со ступенчатым энергетическим прерыванием.